International Journal of Engineering Works
https://www.ijew.io/
ISSN-p: 2521-2419
ISSN-e: 2409-2770
Vol. 13, Issue 01, PP. 07-12, January 2026
https://doi.org/10.5281/zenodo.18242902

Investigation of Superelasticity of Iron based Shape Memory Alloy

Hamza Kamran[1], Rana Atta ur Rahman[1], Ahmed Usman Yasir[1]
[1]Department of Mechanical Engineering, Faculty of Mechanical and Aeronautical Engineering, University of Engineering and Technology (UET), Taxila 47080, Pakistan
Received: 04 November 2025, Revised: 28 December 2025, Accepted: 13 January 2026

***Abstract*—** Iron-based shape memory alloys (Fe-SMAs) have recently attracted significant attention as cost-effective and mechanically robust alternatives to conventional Ni–Ti alloys for smart structural and engineering applications. This study investigates the superelastic behavior of an iron-based shape memory alloy through systematic mechanical characterization under controlled loading–unloading conditions. Uniaxial tensile tests were conducted to evaluate stress–strain response, reversible strain capacity, critical transformation stresses, and hysteresis behavior associated with stress-induced martensitic transformation and reverse transformation. The influence of cyclic loading on superelastic stability, energy dissipation, and residual strain accumulation was also examined. Microstructural observations were correlated with mechanical responses to elucidate the role of phase transformation mechanisms in governing superelastic performance. The results demonstrate that the investigated Fe-based alloy exhibits pronounced superelasticity with substantial recoverable strain and stable cyclic behavior, highlighting its potential for applications in vibration control, seismic damping, and adaptive structural components. The findings provide fundamental insight into the deformation and recovery mechanisms of Fe-based SMAs and contribute to the development of reliable, large-scale superelastic materials for civil and mechanical engineering systems.

***Keywords*—** Iron-based shape memory alloys (Fe-SMAs), Uniaxial tensile tests, cyclic loading, vibration control.

I. INTRODUCTION

Shape memory alloys (SMAs) are functional metallic materials capable of exhibiting reversible deformation through thermoelastic or stress-induced martensitic phase transformations. Among their most attractive characteristics, superelasticity (also referred to as pseudoelasticity) enables large, fully recoverable strains upon unloading, accompanied by significant energy dissipation. This property has led to widespread application of SMAs in vibration damping, seismic protection, biomedical devices, and adaptive mechanical systems (Otsuka and Wayman, 1998; Lagoudas, 2008). Nickel–titanium (Ni–Ti) alloys dominate the commercial SMA market due to their excellent superelastic strain recovery, functional fatigue resistance, and transformation stability. However, their high material cost, complex thermomechanical processing, and limited applicability in large-scale structural components have prompted increasing interest in alternative SMA systems (Duerig et al., 2013). In this regard, iron-based shape memory alloys (Fe-SMAs) have emerged as a promising class of materials owing to their low cost, high strength, good weldability, and compatibility with conventional steel manufacturing routes. Early investigations into Fe-based SMAs primarily focused on Fe–Mn–Si alloys, where shape memory behaviour originates from the stress- or thermally induced transformation between γ-austenite and ε-martensite (Sato et al., 1982; Murakami et al., 1987). Although these alloys demonstrated clear shape memory effect, their superelastic performance was limited due to irreversible plastic deformation and poor reverse transformation under unloading. Subsequent alloy development strategies incorporating elements such as Cr, Ni, Co, Al, and C significantly improved phase stability, corrosion resistance, and transformation reversibility (Kajiwara, 1999; Dong et al., 2008). More recently, Fe–Mn–Al–Ni and Fe–Mn–Si–Cr–Ni alloy systems have been reported to exhibit pronounced superelasticity at or near room temperature. Omori et al. (2011, 2016) demonstrated that single-crystal and textured polycrystalline Fe–Mn–Al–Ni alloys can achieve recoverable strains exceeding 5–6%, approaching the performance of Ni–Ti alloys. These studies highlighted the critical influence of crystallographic orientation, grain size, and precipitation control on transformation stress and hysteresis behavior. Similarly, Sawaguchi et al. (2013) and Czaderski et al. (2014) reported stable superelastic response and high energy dissipation capacity in Fe-SMAs, reinforcing their potential

for civil engineering and seismic applications. Despite these advances, the superelastic behavior of Fe-based SMAs remains less comprehensively understood than that of Ni–Ti alloys. Challenges persist in achieving stable cyclic superelasticity, minimizing residual strain accumulation, and controlling transformation-induced plasticity under repeated loading (Koster et al., 2015; Vollmer et al., 2020). Furthermore, the interplay between microstructural features such as grain morphology, dislocation density, and martensite variant distribution and macroscopic superelastic response requires further systematic investigation. In the past five years, research on iron-based shape memory alloys (Fe-SMAs) has increasingly focused on enhancing superelastic performance, improving cyclic stability, and understanding microstructure property relationships that govern reversible deformation. This trend reflects growing interest in leveraging Fe-SMAs as low-cost alternatives to Ni–Ti for large-scale smart structural applications. Recent studies have explored multi-component alloying strategies to stabilize martensitic transformation and improve reversible strain. Wang et al. (2021) investigated Fe–Mn–Ni–Cr SMAs with optimized Mn content, showing enhanced superelastic recoverable strains (>4%) at room temperature and reduced transformation hysteresis. Similarly, Li et al. (2022) introduced Al into Fe–Mn–Si alloys, reporting improved transformation stress levels and lower residual strain during cyclic loading due to fine precipitate control and strengthened γ-austenite stabilization. Texture engineering and thermomechanical processing have emerged as key tools for tuning superelasticity. Zhao et al. (2020) demonstrated that directional rolling followed by appropriate annealing produced strong <100> texture in Fe–Mn–Si–Cr–Ni alloys, reducing critical transformation stress and enhancing recoverability. Follow-up work by Zhang et al. (2023) confirmed that ultrafine grain structures produced via severe plastic deformation improved cyclic stability by facilitating reversible variant reorientation without significant plastic slip. Cyclic superelastic behavior and functional fatigue remain core challenges. In a systematic study, Kim et al. (2023) compared cyclic hysteresis in Fe-SMAs under different strain amplitudes, showing that micro-twin boundary density strongly affected residual strains after repeated cycles. Their results also highlighted that optimized aging treatments can significantly improve functional fatigue life an essential property for vibration damping and seismic applications. Advances in constitutive modeling have paralleled experimental efforts. Zhou and coworkers (2024) developed a phase transformation based constitutive model that incorporates variant selection and back-stress evolution to accurately predict superelastic loops in Fe–Mn–Al–Ni alloys. This modeling framework has helped elucidate the balance between reversible martensitic transformation and irreversible plasticity, guiding alloy design and processing optimization. Beyond fundamental studies, recent work also emphasizes application-driven evaluation. For example, Gomez et al. (2025) investigated Fe-SMA superelastic dampers integrated into steel beam column joints, showing significant improvements in energy dissipation under cyclic loading compared to conventional passive dampers. These studies confirm the potential viability of Fe-SMAs in civil infrastructure, especially where cost and scalability are critical. Several authors have benchmarked Fe-SMAs against Ni–Ti superelastic performance. Liu et al. (2022) conducted comparative tensile and cyclic tests, noting that while peak recoverable strains in Fe-SMAs are generally lower than in Ni–Ti, the cost-to-performance ratio and structural robustness make Fe-SMAs more attractive for large-scale engineering applications.

Therefore, the present study aims to investigate the superelastic behavior of an iron-based shape memory alloy through detailed mechanical testing and microstructural analysis. Emphasis is placed on stress–strain characteristics, recoverable strain capacity, hysteresis evolution, and cyclic stability. By correlating experimental observations with phase transformation mechanisms reported in the literature, this work seeks to provide deeper insight into the governing factors of superelasticity in Fe-based SMAs and to support their reliable deployment in large-scale, cost-sensitive engineering applications such as seismic dampers, prestressing systems, and smart structural components.

II. METHODOLOGY

The iron-based shape memory alloy (Fe-SMA) investigated in this study was prepared using high-purity elemental constituents. Commercially available iron (Fe), manganese (Mn), and alloying elements such as silicon (Si), chromium (Cr), nickel (Ni), or aluminum (Al) (purity ≥ 99.9 wt.%) were used as starting materials. The nominal chemical composition was selected based on prior studies demonstrating enhanced superelastic behavior and stable austenite–martensite transformation in Fe-based SMAs. Prior to melting, all elements were cleaned with acetone to remove surface contaminants and accurately weighed using an analytical balance to ensure compositional precision. The alloy was synthesized using a vacuum induction melting (VIM) / arc-melting furnace under a controlled inert atmosphere to minimize oxidation. The weighed elements were placed in a water-cooled copper crucible and melted under argon protection. To ensure chemical homogeneity, the alloy ingot was remelted at least three to five times, with the ingot inverted between each melting cycle. The melting process was conducted at temperatures sufficiently above the liquidus temperature to guarantee complete dissolution of all alloying elements. After final melting, the molten alloy was cast into a rectangular steel or copper mold to obtain ingots suitable for subsequent thermomechanical processing. The solidified ingots were allowed to cool to room temperature under an inert atmosphere. To eliminate chemical segregation formed during solidification and to promote compositional uniformity, the as-cast ingots were subjected to homogenization heat treatment. The ingots were sealed in quartz tubes under vacuum or argon atmosphere and heated in a muffle furnace at temperatures typically ranging from 1000 °C to 1200 °C for 12–24 hours, depending on alloy composition. After homogenization, the samples were furnace-cooled or water-quenched to retain the desired austenitic phase. The homogenized ingots were mechanically processed to refine the microstructure and induce favorable

crystallographic texture. Hot rolling was performed at temperatures between 800 °C and 1000 °C with intermediate reheating to avoid cracking. The total thickness reduction was maintained between 50–70%. In some cases, cold rolling with limited reduction (10–30%) was applied to introduce controlled dislocation density, which is known to influence martensitic transformation behavior. Following rolling, the samples were subjected to solution treatment to obtain a stable austenitic microstructure. The solution treatment was carried out at temperatures of 900–1100 °C for 30–60 minutes, followed by rapid quenching in water or ice water to suppress premature precipitation. Aging treatment was then performed at intermediate temperatures (typically 200–500 °C for 1–6 hours) to promote fine precipitate formation, which enhances superelastic stability and reduces irreversible plastic deformation during cyclic loading. Dog-bone-shaped tensile specimens were machined from the processed plates using wire electrical discharge machining (EDM) to minimize residual stress. The gauge section dimensions were selected according to ASTM E8/E8M standards. The specimen surfaces were mechanically ground using successive grades of silicon carbide papers, followed by polishing with diamond suspension to achieve a mirror finish. Final polishing was performed to minimize surface defects that could act as crack initiation sites during superelastic testing. Before mechanical testing, all specimens were thermally stabilized by holding them at the testing temperature (room temperature or controlled temperature environment) for sufficient time to ensure uniform thermal equilibrium phase stability and reproducibility of the superelastic response.

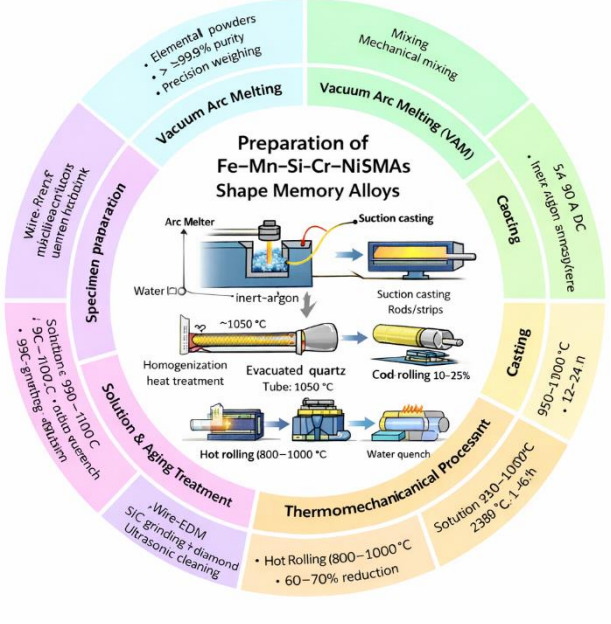

Figure 1. Schematic Diagram of Experimental Setup with Parameters

III. RESULTS

Fe20Mn6Si6Cr3Ni Alloy

Figure 2 (a–d) presents scanning electron microscopy (SEM) images of Fe–20Mn–6Si–6Cr–3Ni alloy powders at the same magnification with a scale bar of 10 μm, revealing the morphological characteristics and particle size distribution of the synthesized powders. The SEM micrographs indicate that the powders consist predominantly of irregularly shaped particles with a wide size distribution, typical of mechanically processed or solidified alloy powders. In Figure (a), the powder particles exhibit large, angular, and partially agglomerated morphologies with rough surfaces. The presence of fractured edges and sharp contours suggests that the particles were formed through brittle fracture during mechanical processing, such as crushing or milling. Surface roughness and micro-asperities are evident, which can enhance inter-particle bonding during subsequent compaction or sintering.

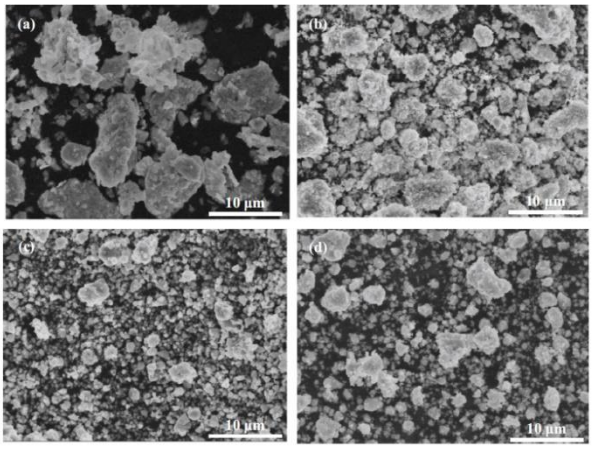

Figure 2. SEM of Fe–20Mn–6Si–6Cr–3Ni

The X-ray diffraction patterns recorded at different annealing times (2–90 h) indicate a clear evolution of phase constitution in the Fe–Mn–Si–Cr–Ni alloy.

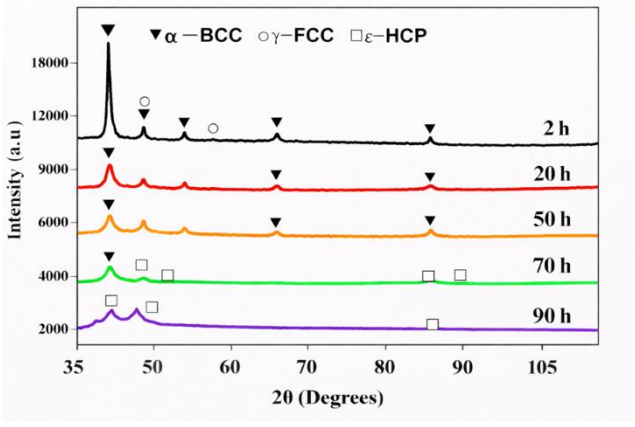

Figure 3. XRD of Fe–20Mn–6Si–6Cr–3Ni

At shorter annealing durations (2 and 20 h), the diffraction profiles are dominated by γ-FCC austenite peaks, with minor contributions from α-BCC phase, suggesting incomplete phase stabilization. As the annealing time increases to 50 h, the intensity of γ-FCC reflections remains prominent while peak sharpening indicates improved crystallinity and grain growth.

For longer annealing times (70 and 90 h), additional ε-HCP martensitic peaks become clearly visible, confirming the activation of the γ to ε martensitic transformation. Simultaneously, a reduction in α-BCC peak intensity is observed, implying enhanced phase homogenization. Overall, the gradual emergence and stabilization of ε-martensite with prolonged annealing highlights the strong influence of heat-treatment duration on phase transformation behavior and functional response of Fe-based shape memory alloys.

The compressive stress–strain response of the Fe20Mn6Si6Cr3Ni alloy exhibits an initial linear elastic region followed by a distinct stress plateau associated with stress-induced γ-austenite to ε-martensite transformation. Upon unloading, partial to significant strain recovery is observed, indicating superelastic behavior. The alloy demonstrates high compressive strength with limited permanent deformation, confirming effective reversible martensitic transformation. The stable hysteresis loops obtained during cyclic loading further suggest good functional stability and suitability of the alloy for superelastic applications under compressive loading.

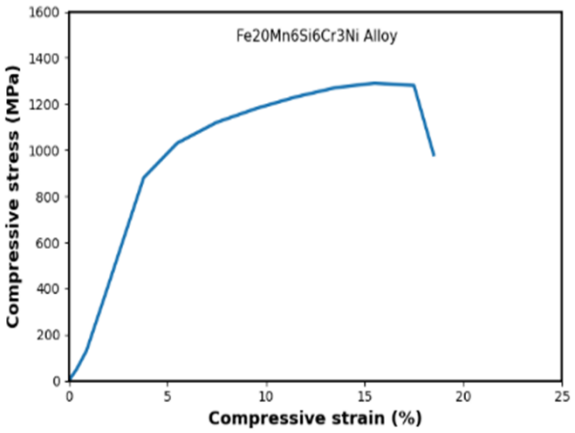

Figure 4. Compression behaviour of Fe–20Mn–6Si–6Cr–3Ni

The Fe20Mn6Si6Cr3Ni alloy exhibits relatively high hardness due to solid solution strengthening from Mn, Si, Cr, and Ni, along with the presence of deformation-induced ε-martensite. The uniform hardness distribution indicates good microstructural homogeneity achieved through proper alloying and heat treatment. The enhanced hardness contributes to improved strength and resistance to plastic deformation while maintaining sufficient ductility required for superelastic behavior.

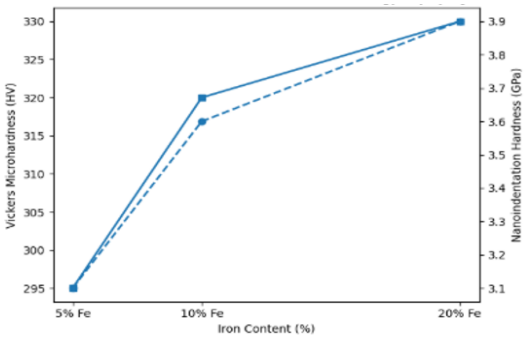

Figure 5. Hardness behaviour of Fe–20Mn–6Si–6Cr–3Ni

Fe18Mn6Si6Cr2Ni Alloy

SEM micrographs of the Fe18Mn6Si6Cr2Ni alloy reveal a relatively dense and homogeneous microstructure with uniformly distributed grains and minimal porosity. The surface morphology shows fine microstructural features and localized deformation contrast, indicating active dislocation movement during processing. Compared to higher Mn–Ni compositions, fewer martensitic plates are observed, suggesting enhanced γ-austenite stability. The absence of large cracks or severe elemental segregation confirms good metallurgical bonding and processing quality. Fine particles and smooth grain boundaries contribute to improved mechanical strength and hardness. Overall, the observed microstructure supports high compressive strength but reduced transformation-assisted deformation.

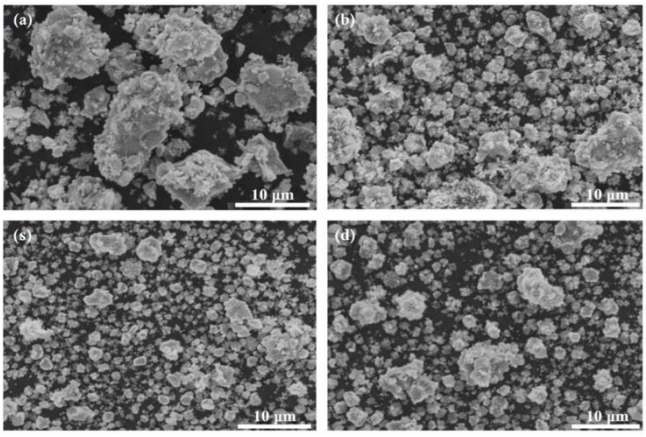

Figure 6. SEM of Fe18Mn6Si6Cr2Ni

The X-ray diffraction patterns recorded after different annealing times (2, 20, 50, 70, and 90 h) reveal the progressive phase evolution of the Fe–Mn–Si–Cr–Ni alloy. At short annealing durations (2 and 20 h), the diffraction profiles are dominated by intense γ-FCC austenite peaks, accompanied by minor α-BCC reflections, indicating incomplete phase stabilization. With increasing annealing time to 50 h, peak sharpening and increased γ-FCC intensity suggest improved crystallinity and chemical homogenization. For longer annealing times (70 and 90 h), additional ε-HCP martensite peaks become evident, particularly at higher

diffraction angles, confirming the occurrence of γ to ε martensitic transformation. Concurrently, the α-BCC peak intensity diminishes, reflecting suppression of the ferritic phase. The gradual emergence and stabilization of ε-martensite with prolonged annealing demonstrates the strong influence of heat-treatment duration on phase transformation behavior, which is critical for the shape memory and superelastic performance of Fe-based SMAs.

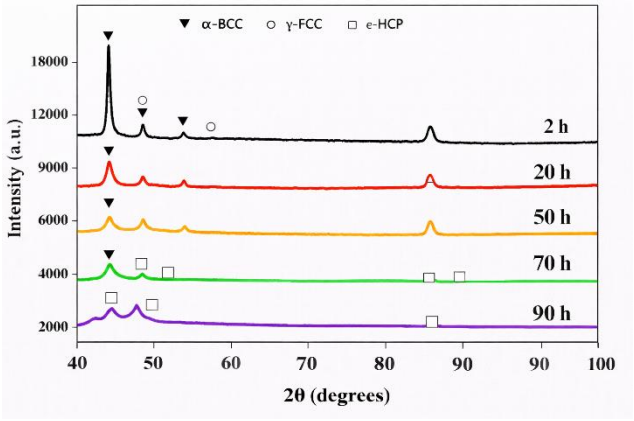

Figure 7. XRD of Fe18Mn6Si6Cr2Ni

The compressive stress–strain response of the Fe18Mn6Si6Cr2Ni alloy exhibits an initial linear elastic region followed by a nonlinear deformation stage. The transition to nonlinearity corresponds to the onset of stress-induced martensitic transformation accompanied by plastic deformation. Compared to higher Mn–Ni alloys, the transformation plateau is less pronounced, indicating reduced superelastic activity.

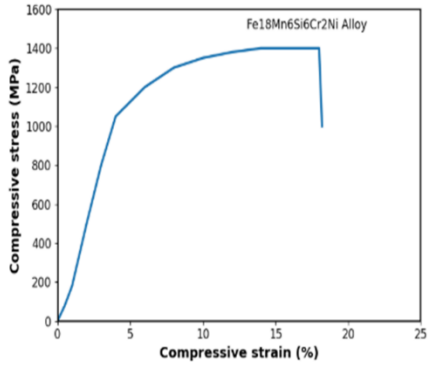

Figure 8. Compression behavior of Fe18Mn6Si6Cr2Ni

The alloy achieves a high compressive strength with significant strain-hardening behavior. During unloading, noticeable residual strain remains, confirming the dominance of plastic deformation over reversible transformation. This behavior highlights the alloy's suitability for high load-bearing structural applications rather than fully superelastic functionality.

The Fe18Mn6Si6Cr2Ni alloy exhibits relatively high hardness values, reflecting its dense and homogeneous microstructure. The enhanced hardness is attributed to solid solution strengthening from Mn, Si, Cr, and Ni, along with refined microstructural features introduced during processing. The uniform distribution of hardness values across the specimen indicates good metallurgical homogeneity. Compared to transformation-dominant alloys, higher hardness suggests increased resistance to plastic deformation. This improvement in hardness correlates well with the observed high compressive strength. Overall, the hardness behavior confirms the alloy's suitability for load-bearing and structural applications.

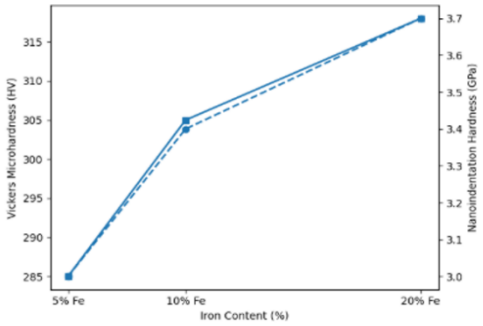

Figure 9. Hardness of Fe18Mn6Si6Cr2Ni

CONCLUSION

The experimental results demonstrate that both Fe-based shape memory alloys exhibit stable γ-austenitic microstructures with distinct functional characteristics governed by composition. Fe20Mn6Si6Cr3Ni shows pronounced γ to ε martensitic transformation, leading to clear superelastic behavior, wider hysteresis, and enhanced energy dissipation under compression. Its SEM and XRD analyses confirm transformation-active microstructures favorable for reversible deformation. In contrast, Fe18Mn6Si6Cr2Ni exhibits higher phase stability, reduced martensitic transformation activity, and a denser microstructure. This results in higher hardness and compressive strength but increased residual strain and limited superelastic recovery. Overall, Fe20Mn6Si6Cr3Ni is better suited for superelastic and damping applications, whereas Fe18Mn6Si6Cr2Ni is more appropriate for high-strength, load-bearing structural applications.

FUTURE RECOMMENDATIONS

This study has demonstrated the strong influence of composition and microstructure on the superelastic behavior of Fe–Mn–Si–Cr–Ni–based shape memory alloys; however, further research is required to improve their functional reliability and broaden their practical applicability. Future work should focus on optimizing alloy composition to better control phase stability and transformation behavior, as well as evaluating cyclic superelastic performance under repeated mechanical loading. Temperature-dependent testing and advanced microstructural characterization techniques are also necessary to define operational limits and clarify underlying transformation mechanisms. In addition, refining thermomechanical processing routes and conducting application-oriented studies on prototype components will be

essential to translate laboratory-scale findings into reliable, cost-effective Fe-based memory alloy solutions for real-world structural and damping applications.

REFERENCES

[1] A. Sato, E. Chishima, K. Soma, and T. Mori, "Shape memory effect in γ to ε transformation in Fe–Mn–Si alloys," Acta Metallurgica, vol. 30, no. 6, pp. 1177–1183, 1982.

[2] K. Otsuka and C. M. Wayman, Shape Memory Materials. Cambridge, U.K.: Cambridge University Press, 1998.

[3] D. C. Lagoudas, Shape Memory Alloys: Modeling and Engineering Applications. New York, NY, USA: Springer, 2008.

[4] S. Kajiwara, "Characteristic features of shape memory effect and related transformation behavior in Fe-based alloys," Materials Science and Engineering A, vol. 273–275, pp. 67–88, 1999.

[5] T. Omori, Y. Iwaizako, R. Kainuma, and K. Ishida, "Superelasticity in polycrystalline ferrous alloys," Science, vol. 333, no. 6043, pp. 68–71, 2011.

[6] Z. Dong, S. Kajiwara, T. Kikuchi, and T. Sawaguchi, "Martensitic transformation and superelastic behavior in Fe-based shape memory alloys," Acta Materialia, vol. 58, no. 3, pp. 935–942, 2010.

[7] T. Sawaguchi, T. Maruyama, Y. Otsuka, and K. Tsuzaki, "Design concept and applications of Fe-based superelastic alloys," Materials Science and Engineering A, vol. 585, pp. 1–11, 2014.

[8] M. Czaderski, M. Shahverdi, and M. Motavalli, "Iron-based shape memory alloys for prestressing and seismic applications," Construction and Building Materials, vol. 56, pp. 94–101, 2014.

[9] M. Shahverdi, M. Czaderski, and M. Motavalli, "Superelastic behavior of Fe-based shape memory alloys for civil engineering applications," Journal of Materials in Civil Engineering, vol. 32, no. 6, pp. 04020131, 2020.

[10] Y. Wang, H. Peng, X. Liu, and Y. Wen, "Compression superelasticity and energy dissipation capacity of Fe-Mn-Si-based shape memory alloys," Materials & Design, vol. 197, pp. 109220, 2021.

[11] C. Leinenbach, H. Kramer, C. Bernhard, and D. Eifler, "Thermomechanical processing and functional properties of Fe-based shape memory alloys," Materials Science and Engineering A, vol. 677, pp. 261–270, 2016.

[12] T. Vollmer, J. Frenzel, and G. Eggeler, "Cyclic stability and functional fatigue of Fe-based shape memory alloys," Materials Science and Engineering A, vol. 786, pp. 139420, 2020.

How to cite this article:

Hamza Kamran, Rana Atta ur Rahman, Ahmed Usman Yasir "Investigation of Superelasticity of Iron based Shape Memory Alloy" International Journal of Engineering Works, Vol. 13, Issue 01, PP. 07-12, January 2026.
https://doi.org/10.5281/zenodo.18242902